

Chaotic three-dimensional distribution of Ba, Rb, and Sr in feldspar megacrysts grown in an open magmatic system

Ewa Słaby · Michał Śmigielski · Tomasz Śmigielski ·
Andrzej Domonik · Klaus Simon · Andreas Kronz

Received: 9 August 2010 / Accepted: 25 March 2011 / Published online: 19 April 2011
© The Author(s) 2011. This article is published with open access at Springerlink.com

Abstract As has been demonstrated in recent years, the heterogeneities of coeval magmas can be more successfully revealed by zoned megacrysts rather than by analysis of the whole rocks hosting them. Here, the geochemical heterogeneities of feldspar megacrysts from the Karkonosze granite, Poland, are investigated by LA-ICP-MS. The crystals are the product of migration and growth in regions of poorly mixed magmas. 3D-modeling of the Ba, Sr, and Rb distributions emphasizes the importance of micro-domain growth morphologies. Two models of element behavior—a relative concentration model and a composition gradient

model—provide a potentially effective tool for tracking the mixing process on a microscale. Measured concentrations of elements of different mobilities do not agree with what might be expected from the mixing of two end-member magmas. If mixing was the only process occurring, linear correlations between the concentrations of any two elements should be observed; this, however, is not the case. For combinations of any two of the three elements, modeling reveals differing non-linear correlations between concentrations. The megacryst heterogeneities provide an insight into how mixing magmas are chaotically advected to growing crystals and the degree of inter-magma element exchange between the magmas.

Communicated by J. Hoefs .

Electronic supplementary material The online version of this article (doi:10.1007/s00410-011-0631-6) contains supplementary material, which is available to authorized users.

E. Słaby (✉)

Institute of Geological Sciences, Polish Academy of Sciences,
Research Centre in Warsaw, Twarda 51/55, 00-818 Warsaw,
Poland
e-mail: e.slabby@twarda.pan.pl

M. Śmigielski

Institute of Geology, University of Warsaw, Żwirki i Wigury 93,
02-089 Warsaw, Poland

T. Śmigielski

‘Sofrecom Polska’, Grójecka 5, 02-019 Warsaw, Poland

A. Domonik

Institute of Hydrogeology and Engineering Geology, University
of Warsaw, Żwirki i Wigury 93, 02-089 Warsaw, Poland

K. Simon · A. Kronz

Department of Geochemistry, GZG of Georg-August-University,
Goldschmidtstrasse 1, 37077 Göttingen, Germany

Keywords Mixing · Element mobility · Diffusion ·
Alkali feldspar · 3D-depiction · Cut-off value models ·
Gradient models · Probabilistic models ·
Geochemical heterogeneity · Karkonosze granite

Introduction

Magma mixing is a process commonly considered to trigger extreme geochemical heterogeneities on both the macro- and microscale (e.g., Barbarin 2005; Bonin 2004; Pietranik and Koepke 2009; Poli et al. 1996; Słaby et al. 2008a; Tepley et al. 2000; Waight et al. 2000 among many). On the macro-scale, the chaotic dynamics of the process are registered in rock geochemistry and textures. It is commonly accepted that if mixing is the only process occurring in the system, linear correlations between the concentrations of any two elements should result. The process has been simulated using a linear equation combining the composition of the two end-member magmas, that of the hybrid, and the progress of the mixing process

(Fourcade and Allegre 1981; Langmuir et al. 1978)—an equation that has been used in many publications.

An important new step in the understanding of the complex nature of magma mixing and its macro-scale description was the coupled application of chaos theory and fractal geometry with geochemistry (De Rosa et al. 2002; Ferrachat and Ricard 1998; Flinders and Clemens 1996; Perugini and Poli 2004; Perugini et al. 2002; Perugini et al. 2003; Poli and Tommasini 1991). In contrast to the Langmuir et al. (1978) view, simulation of the chaotic dispersion of one magma in another requires use of a non-linear equation (Liu et al. 1994a, b; Mandelbrot 1982; McCauley 1993; Ottino et al. 1993). The highly non-linear character of the mixing process has also been revealed by experimental simulation (Bindeman and Davis 1999; De Campos et al. 2004, 2008, 2010; García-Moreno et al. 2006; Kouchi and Sunagawa 1984; Perugini et al. 2008).

The microscale can be clearly recognized in mineral compositions and growth morphologies (Gagnevin et al. 2005; Ginibre et al. 2004; Pietranik and Koepke 2009; Słaby and Götze 2004; Słaby et al. 2007a, b, 2008a, b; Tepley et al. 2000; Waight et al. 2000). Induced by mixing, crystal growth progresses in an environment where the dispersion of magmas proceeds by chaotic stretching and folding (Liu 1994b; Perugini and Poli 2004; Perugini et al. 2002; Perugini et al. 2003). As a result, magma domains with differing characteristics may occur simultaneously and/or sequentially close to the growing mineral surface, and elements from all domains are incorporated due to their advection and diffusive fractionation (Perugini et al. 2006). Some examples of the deterministic nature of crystal growth have been analyzed and tested (Holten et al. 1997; Perugini et al. 2005; Słaby et al. 2008b).

The crystallization history of a mineral is typically revealed by its zoned trace-element distribution pattern. A three-dimensional depiction of such a trace-element distribution in a cross-cut of a single feldspar zone, formed during intensive stirring of two magmas of contrasting compositions, shows a complex pattern of domains variably enriched and impoverished (Słaby et al. 2008a). The binary diagrams exhibit linear correlation for some elements in the crystal and deviation from such in others, supporting and questioning the adequacy of the linear equation for describing the ongoing process on a micro-scale. Assuming the mixing process and the associated chemical exchange to be time dependent, the dynamic of the advection–diffusion process should differ for elements with clearly different rates of diffusion during exchange on a short time scale. Due to the different diffusivities of elements in the melts, their exchange between magma domains progresses at different rates, thus increasing the inhomogeneity of the domains. As the process is time

dependent, the concentration patterns in the domains change as the process advances.

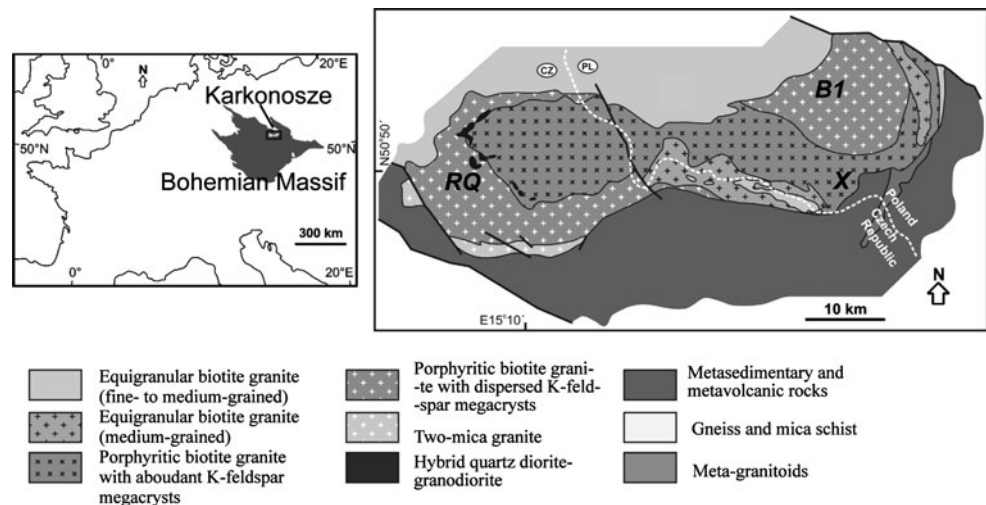
The aim of this study was to introduce new tools for the in-depth interpretation of trace-element distributions in heterogeneous mineral domains formed during mixing and to correlate these distributions with progressive equilibration as heterogeneous domains become more coherent due to magma homogenization. 3D depictions and related digital models of element distribution patterns along with models of mutual relations between the patterns open new perspectives for such studies and demonstrate that mixing does not show linear trace-element behavior during exchange. They can also give insight into the proportions of active- and coherent magma domains in a magmatic field at a given stage of crystal formation. For this study, feldspars representing different degrees of magma blending (being mixtures of two end-member mafic and felsic melts) were selected from a single pluton. As the process is likely to be best developed and registered in feldspar domains grown in regions in which magmas mixed intimately, such domains were the foci for feldspar selection.

Sample selection

The alkali feldspars were collected from the composite Karkonosze pluton of A-granite affinity in SW Poland (Fig. 1). This pluton was mainly derived by mixing of crustal felsic magma (of weakly peraluminous character) with mafic (lamprophyric) magmas injected over time from an enriched mantle source (Słaby and Götze 2004; Słaby and Martin 2008). The process is reflected in a succession comprising hybridized porphyritic granite, hybridized granodiorites, intermediate enclaves in granite and subsequent composite- and late mafic dykes. Granite free of contamination, representing a pure crust-related magma, occurs as an equigranular facies.

Every member of this succession resulted from differing degrees of inter-magma viscosity contrast and might be related to an individual stage of replenishment in the granite chamber. In addition, the geochemical data indicate that both felsic- and mafic magmas evolved independently by fractional crystallization. Thus, the succession reveals that mixing occurred in a chamber episodically replenished by mafic magma of varying composition that interacted with felsic magma also of varying composition. The models developed by Słaby and Götze (2004), Słaby et al. (2007a, b), and by Słaby and Martin (2008) indicate at least three stages of mixing, each involving different end-member magma compositions. Such an interaction implies a long-lived mafic magma source coexisting with a granitic chamber and argues for a deep-seated mafic magma chamber rather than for continuous mantle melting.

Fig. 1 The Karkonosze pluton within the Bohemian Massif and a map of the pluton and its metamorphic envelope (after Žák et al. 2008). *RQ*, *B1*, *X*—sample localities



Geochemical modeling of the evolution of the pluton (Słaby and Martin 2008) is compatible with the emplacement sequence of Žák and Klomínský (2007) and Žák et al. (2008, 2009).

The feldspar crystals collected represent the feldspars in hybrid granodiorite (*RQ*—Rudolfov quarry), feldspars mechanically introduced into microgranular mafic enclaves (*B1*—Bukówka Hill) and those in porphyritic hybrid granite (*X*—Karpacz). Sample locations are shown in Fig. 1.

Feldspar growth in active (AR) and coherent (CR) magma regions

Basic principles

The advection/diffusion models of Perugini et al. (2002, 2003, 2005) suggest that at any given time, growing feldspar zones reflect the composition of the magma in their immediate environs. In their model simulation of the mixing process (Fig. 2; Perugini et al. 2002), magma regions which preserves pristine, end-member, magma compositions are defined as coherent regions (CR) and those where magmas are intimately mixed, as active regions (AR). During the migration of megacrysts between well-mixed (AR) and poorly mixed regions (CR), their growth is chaotically fed by interaction to varying degrees with both magmas. Migration along each discrete sector of the hypothetical migration path on Fig. 2 results in the crystallization of a zone. During crystal migration through a corresponding real heterogeneous magmatic field, chaotic advection is coupled with chemical exchange (Perugini et al. 2003; 2005). Thus, information about the heterogeneity of coeval magmas retrieved from zoned megacrysts has the potential be more detailed than that obtained from

the whole rocks hosting them, allowing the mixing-mingling process to be traced step by step (Słaby et al. 2007a, b).

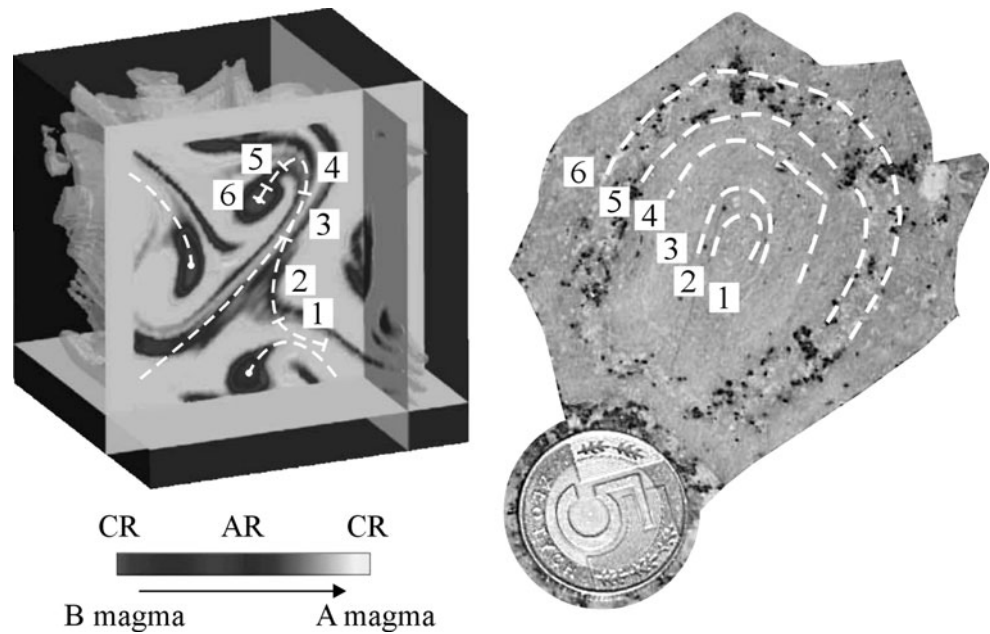
The whole process is self-affine and time dependent, i.e., every segment of the CR–AR pattern developed due to the advancing process should reveal a similar arrangement. Thus, the use of increasingly sensitive tools to reveal the detail of the crystal composition should result in similar relationships between investigated elements, and local configurations ought to demonstrate the increasing complexity of the growth process.

Crystallization process in the Karkonosze pluton

One crucial premise based on the Perugini et al. diffusion/advection model is the assumption that the crystallization of the megacrysts was continuous—that alkali feldspar megacrysts continued to grow as they traversed through mafic/felsic coherent- and active regions. For this to be reasonable, K-feldspar must be an early liquidus phase in both the well-mixed and coherent magma regions. One of the reasons we believe alkali feldspar can be considered as liquidus phase is that it appears in both end-member rocks—in granite ($Or_{91.6}Ab_{8.3}An_{0.1}$) free of contamination by mafic magma and in lamprophyre ($Or_{57.8-9.7}Ab_{47.0-42.0}An_{2.69-0.2}$). The crystals occurring in lamprophyres reveal high-temperature crystallization conditions and are barium rich. Barium expands the K-feldspar stability field to higher temperatures (Morgan and London 2003). In the hybrid rocks, i.e., granodiorite $Or_{54.6-87.0}Ab_{45.1-11.9}An_{0.3-1.1}$, some enclaves $Or_{73.4-84.5}Ab_{26.5-14.8}An_{0.1-0.7}$ and porphyritic granite $Or_{61.0-97.7}Ab_{38.3-2.3}An_{0.3-0.0}$, alkali feldspars occur as megacrysts and as matrix crystals. Matrix-crystal compositions usually compare with those of megacryst rims.

In both megacrysts and matrix feldspars, cathodoluminescence studies revealed two types of zoned growth

Fig. 2 Simulation by Perugini et al. (2002) of the magma mixing process in 3D with likely hypothetical feldspar crystallization paths, one of which is divided into six discrete sectors (*left*), and a feldspar from Karkonosze with a zoned growth texture reflecting migration along an analogous real path. Abbreviations: CR Coherent magma region, AR active magma region. Coin ~24 mm diam



patterns—with or without resorption interfaces and lack of any inherited material from the source region (Słaby and Götze 2004; Słaby et al. 2008a, b). Resorption interfaces point to discontinuity in the crystal growth. However the relationship between compatible and incompatible elements argues against any widespread recrystallization process following dissolution. Even if zones of both types show fluctuating trace-element patterns, these patterns are characterized, as shown by Słaby et al. (2007b, 2008a), by systematic and coupled relationships between incompatible (LREE, Cs) and compatible elements (Ba, Sr, Rb). Such coupling indicates near equilibrium growth conditions. If growth was driven by kinetically controlled processes, the uptake of compatible elements would have been decoupled from that of the incompatible elements (Morgan and London 2003).

Some of the zones appear to have crystallized in a homogenous magmatic environment having clear geochemical affinities with the end-member magmas in the Karkonosze pluton (Słaby et al. 2007b), whereas others crystallized in heterogeneous domains of hybridized magma. Geochemical modeling of megacryst growth revealed that zones that can be related to almost pure mafic end-member magma are rare and their width extremely narrow (Słaby et al. 2007a). Those zones that crystallized in coherent felsic or variably hybridized magma are common.

The Pb isotope signatures of the megacrysts are consistent with mixing between a mantle and a crustal end-member (Słaby et al. 2007b). Using the Kober and Lippolt (1985) model for crust-mantle Pb isotope evolution, the amount of mantle-derived Pb in the feldspar composition can be estimated as 20–40% (Słaby et al. 2007b).

Methods

Geochemistry

LA-ICP-MS method was chosen for the trace-element determination for various reasons. The most important was that even though absolute concentrations can be charged with error, the method allows precise assessment of the relative concentration and Ba/Sr/Rb ratios. The models developed and presented in this paper are based on element concentration ratios. The laser ablates material from the surface. The amount of material ablated differs from sample to standard, from spot (mineral 1) to spot (mineral 2) and even during into a given solid material. The total amount always varies greatly. Concentration is defined as the abundance of an element within substrate. To obtain accurate concentration values, two requirements must be met. As with a normal calibration, a transformation of intensity to concentration by means of NBS610, a standard with about 450 ppm of almost each element, should be done. Secondly, an internal standard element/isotope (^{29}Si) must be used to monitor the varying amount of material ablated. A ratio of any isotope to this internal isotope standard is independent of the amount. Using ICP-MS, the intensity ratios can be measured almost as precisely as the internal reproducibility. Consequently, the ratios are determined with very low error.

Laser ablation mass spectrometry (LA-ICP-MS) was carried out at the Geochemisches Institut, Göttingen University, using a FISIONS VG PQ STE instrument with a VG UV-Microprobe laser system (266 nm). Detailed operating conditions are given in Słaby et al. (2008a, b). Each

K-feldspar megacryst was analyzed along a transect from one margin to the other for ^{23}Na , ^{27}Al , ^{29}Si , ^{39}K , ^{43}Ca , ^{49}Ti , ^{55}Mn , ^{57}Fe , ^{85}Rb , ^{88}Sr , ^{133}Cs , ^{137}Ba , ^{139}La , ^{140}Ce , ^{141}Pr , ^{143}Nd , ^{147}Sm , ^{151}Eu , ^{157}Gd , ^{159}Tb , ^{163}Dy , ^{165}Ho , ^{166}Er , ^{169}Tm , ^{172}Yb , and ^{175}Lu . Elemental concentrations were calculated using NBS610 for calibration and ^{29}Si as an internal standard. The counting statistics for Ba, Sr, and Rb show the smallest relative standard deviations of all measured trace elements. Errors for the Ba, Sr, and Rb data are 3–7% standard deviation, for others (incompatible elements), a few tens of percent. At the same time, the ratios of Ba/Sr/Rb were estimated with an error of less than 3% with the very high probability that any overestimation or underestimation, if such occurred, affects all elements in the same manner.

Along the same transects, crystals were profiled by microprobe point analysis in 10–20 μm steps to test the accuracy of the LA-ICP-MS trace-element (Ba) data (Electronic Supplement Fig. 1). Major element (Na, Al, Si, K, Ca) contents were also determined by microprobe point analysis. Thin-section Ba, Na, K, and Ca maps were made using 15 kV accelerating voltage, beam current 100 nA, 20 μm steps, dwell time 40 ms, and beam diameter 10 μm . The analyses were performed using a JEOL JXA 8900 RL microprobe at the Geochemisches Institut, Göttingen University.

Wavelength of analyzed processes

Barium thin-section maps created for the selected feldspars reveal their zoned growth textures. The thickness of the zoning varies from crystal to crystal, but on average, every single major zone exceeds ca 0.75–1.0 mm. Thus, on average, the wavelength of the major geochemical change in the composition of analyzed feldspars, expressed as the thickness of two neighboring zones, is greater than 1.5–2 mm. In this paper, the focus is on changes in Ba/Sr/Rb distributions and their mutual relations in different zones. The K-feldspar megacrysts were analyzed in 250–500 μm steps along transects from one margin to the other in the direction of crystal growth (across zoning). The distance between spots was driven by the wavelength of the change in geochemical composition. The aim was to have on average more than 1.5 sampling spots per zone (Table 1).

Data interpolation and depiction

The main reason for interpolation of data was to generate continuous maps and 3D surface models of element distribution. These models, although affected by interpolation uncertainties, allow the recognition of texture pattern and the qualitative analysis of element distribution using

Table 1 Amount of data and relation between zones, spots and wavelength used for conceptual models of analyzed feldspars

Sample	Data	Element	Zones	Waves	Spots	Spots per zone
B1	2226	Ba	7	3.5	14	2
		Sr	7	3.5	14	2
		Rb	8	4	14	3.50
RQ	1253	Ba	8	4	25	3.13
		Sr	13	6.5	25	1.92
		Rb	14	7	25	1.79
X1	2146	Ba	13	6.5	24	1.85
		Sr	15	7.5	25	1.67
		Rb	15	7.5	25	1.67
X2	1970	Ba	9	4.5	22	2.44
		Sr	11	5.5	22	2
		Rb	10	5	22	2.2
X3	3053	Ba	19	9.5	34	1.79
		Sr	19	9.5	34	1.79
		Rb	21	10.5	34	1.62
X4	2694	Ba	15	7.5	30	2
		Sr	16	8	30	1.88
		Rb	17	8.5	30	1.76

Digital Elevation Model analytical techniques. Natural neighbor interpolation (Sibson 1981) was applied to the data. In doing so, anisotropy in the distribution of the data (zoning) was taken into account. The resolution of models along transect lines is from 100 to 250 μm ; as few as 1–4 columns were added and interpolated between laser spots. The depth resolution of the models is 5 μm , the same as the original data collected (no interpolation). The depiction of the data as a contour maps and surface models of element distribution involved the use of Surfer 8.0 (Golden Software), classical izoline maps, and 3D models merged with shaded relief images (Yoeli 1965). Depiction of the models was preceded by a spline smoothing procedure without any recalculation of the model. The procedure does not affect the distribution or the value of data but provides enhanced images of higher resolution which greatly helps the recognition of texture patterns. Models obtained in this way show hypothetical averaged trace-element distributions in cross-sections through crystals parallel to transect line and to about 450 μm in depth. Models present both first order changes in geochemical composition across zoning and, in depth, changes in element patterns in different zones.

Figure 3a illustrates the method used to depict the data. The LA-ICP-MS spots are located along a traverse (X axis). In depth, change in element distribution is presented in along the perpendicular Y-axis. Element content is presented using a color scale or/and as a third dimension of the surface (Z axis). To further improve the resolution of the data depiction and to best display the spatial distribution of an

element concentration, the vertical scale on the plots was arbitrarily chosen. Different directions of lighting of shaded relief images were used in analyzing various aspects of the morphology of the surface (Cooper 2003). Each laser ablation pulse (60–120 μm in diameter) gives data collected from a 5- μm thick layer of feldspar. A measurement lasting 20 ms per isotope gives 10,000 counts with a counting noise of $\text{SQR}(10,000) = 100$. This measurement, repeated every 0.943 s, provides a complete chemical analysis of a volume of feldspar 5 μm deep and 60–120 μm in diameter. The next analysis, ablating the same amount of feldspar, does not mix with the one before as the aerosol is removed by the carrier gas within 1 s. Thus, the observed variation with depth (Z axes) for a single spot is not an artifact. About 70–100 impulses were used within one spot; the number of laser impulses and the depth reflects the duration of each LA-ICP-MS analysis (Y axes). Some changes in the Y-axis scale were introduced to accommodate disproportions between distances. These, and differences in resolution along the X and Y axes, were taken into account when interpreting the data.

Feldspar heterogeneity

The chosen feldspars represent three different stages of magma mixing and blending. The compatible elements Ba, Sr, and Rb were selected for this study of feldspar growth. In terms of these elements, mixing occurred between mafic lamprophyric magma enriched in barium and strontium and impoverished in rubidium, and felsic magma with the opposite characteristics (Słaby and Götze 2004; Słaby et al. 2007a, Słaby and Martin 2008). In whole rocks, barium is positively correlated with strontium but negatively with

rubidium. The trends are linear and consistent (Słaby et al. 2008a). Important are the absolute values of the chosen elements in end-member mantle and crust-related magmas, respectively 1600/800/150 and 80/20/350. Whereas Ba and Sr concentrations vary by 20–40 times between end-member magmas, the concentration of Rb varies by less than 3 times.

RQ: Feldspar from hybrid granodiorite

The early hybrid granodiorite (RQ) originated from the mixing of two magmas that were in the process of differentiating and were partly crystallized. In terms of chemical exchange of the elements between mafic and felsic magma domains, the mixing process is advanced, but far from completion (Słaby et al. 2007a, b). The alkali feldspar collected from Rudolfov quarry is surrounded by a thin plagioclase mantle—rapakivi texture; this is reflected in the distribution of major elements (Fig. 3b). The feldspar shows Ba zoning (Fig. 3). Using barium as a mixing index, it can be concluded that the feldspar nucleated in magma rich in a felsic component. Later barium-rich zones reveal at least two growth events in magma rich in a mafic component. LA-ICP-MS data were collected mainly along a zone that crystallized in an active magma region (Fig. 3a). The 3D depiction of the observed variation with depth gives evidence of very heterogeneous barium distribution within this zone. The spatial distributions of strontium and rubidium do not repeat the barium pattern (Fig. 6). Although strontium is concentrated in the same zone as barium, its pattern divides into two subzones. Rubidium shows a very different, irregular, and complicated pattern.

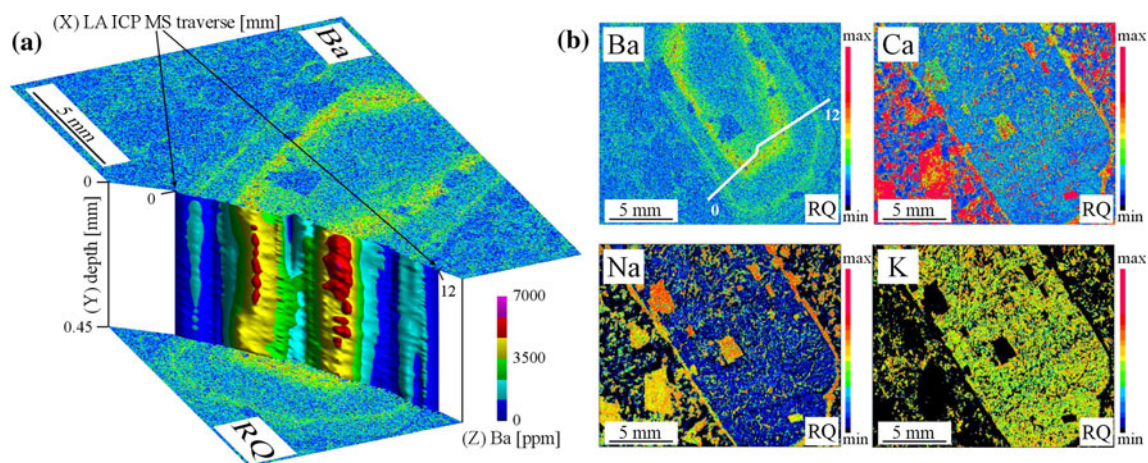


Fig. 3 Major- and trace-element composition of feldspar RQ (collected from early hybridization event). **a** 3D model of spatial distribution of Ba (for Sr and Rb distribution pattern, see Fig. 6). Note highly changeable and irregular inward Ba pattern within the Ba-rich

zone. Axes: X—length of LA-ICP-MS traverse, Y—number of laser impulses, i.e., depth and duration of analysis (1 s to 5 μm), Z—element concentration. **b** Thin-section maps of Ba, Ca, Na and K

B1: Enclave feldspar

The feldspar from enclave (B1) crystallized in felsic magma of end-member composition before being mechanically introduced into the mafic hybrid magma in which its growth was completed. As is feldspar RQ above, this megacryst is homogeneous in terms of major element distribution; zoning is revealed by trace elements. The margin of the feldspar is a broad zone variably enriched in barium that grew in an active magma region after the feldspar had been incorporated into a blob of hybridized mafic magma of almost end-member composition. Inner zones, and a thin outer zone, are evidence of multiple feldspar migrations between AR and CR felsic regions. The data collected along the marked transect on the thin-section barium map are depicted in Fig. 4.

The spatial distribution pattern differs from that of the RQ sample. Enriched- and barren zones are strongly separated. Within the Ba-rich zone, barium shows a heterogeneous pattern of variably enriched- and impoverished domains. The whole area is bordered by a region of barren zones. The pattern is almost perfectly replicated by strontium. Unlike strontium, rubidium occurs in marginal zones poor in barium. Rubidium gathered inboard nearby partly overlaps the Ba and Sr configurations.

X: Granite feldspar

Feldspar X, from porphyritic granite, shows the most advanced mixing going to full completion between two hybrid magmas. One is enriched in crustal-, the other in

mantle-derived components, and both far from end-member composition. The chemical exchange between both magmas is extensive, the degree of blending marked. Fractions of both magmas were almost equal. In contrast to both previous feldspars, X is not a single crystal; it shows a complicated syneusis texture (Fig. 5a). The thin-section Ba map reveals that at least three crystals merged and continued growing together. The merged crystals are simply zoned. Their overgrowth pattern is also zoned but in an irregular and complex manner. Crystal regions enriched in barium are also rich in potassium.

In this case, the whole compound feldspar was separated and cut into parallel slices one above the other and labeled X1, X2, X3, and X4 (Fig. 5b). In all slices, the affinity of barium with strontium is less clear (Fig. 5c–d). Overall, repeating element patterns in the various slices vary in degree. In some slices (e.g., X3; not shown), the patterns of Ba and Sr almost equate; in others, they differ significantly. Rubidium displays little affinity with Ba and Sr (Fig. 5e).

Relative advection/mobility rate: concentration output model

The element distributions presented above are the input data for an output model constructed to analyze the mutual behavior of any two elements and their relative advection–diffusion rates during crystal growth. The relationship between the distribution patterns of two elements should reveal whether locally increased and reduced concentration values for the chosen elements correspond in both patterns

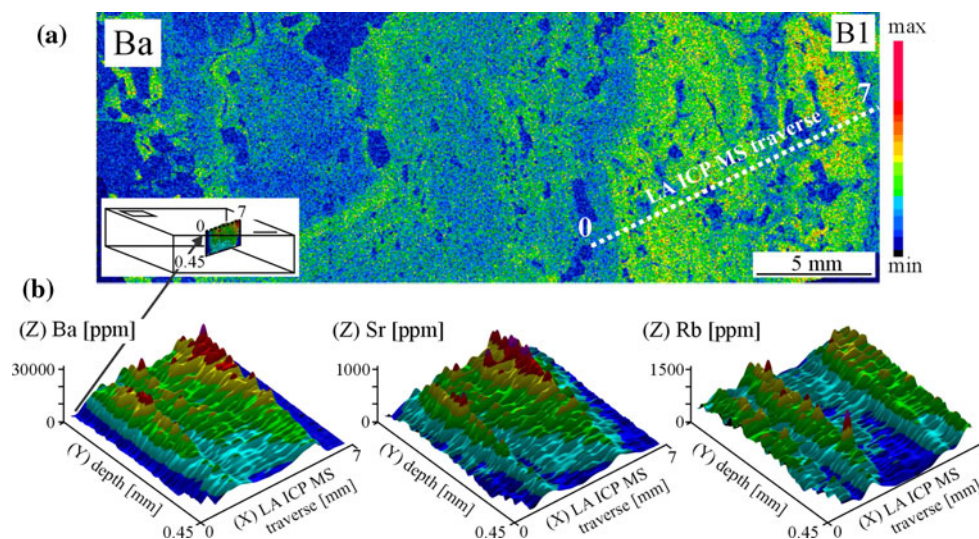


Fig. 4 Trace-element composition of feldspar B1 (enclave feldspar). **a** Ba thin-section map; *white dotted line* and inserted *block-diagram* show LA-ICP-MS transect. **b** The similar patterns of Ba and Sr distribution at depth along the transect are partly overlapped by the Rb pattern. Magma (whole rock) composition shows positive linear

correlation between Ba and Sr and negative correlations for both of them with Rb. Even if Ba and Sr can be related to the composition of coherent-active magma regions, Rb does not suit it. Axes X, Y and Z are as in Fig. 3. *Gray arrow* shows position of the trace of the transect on the thin section

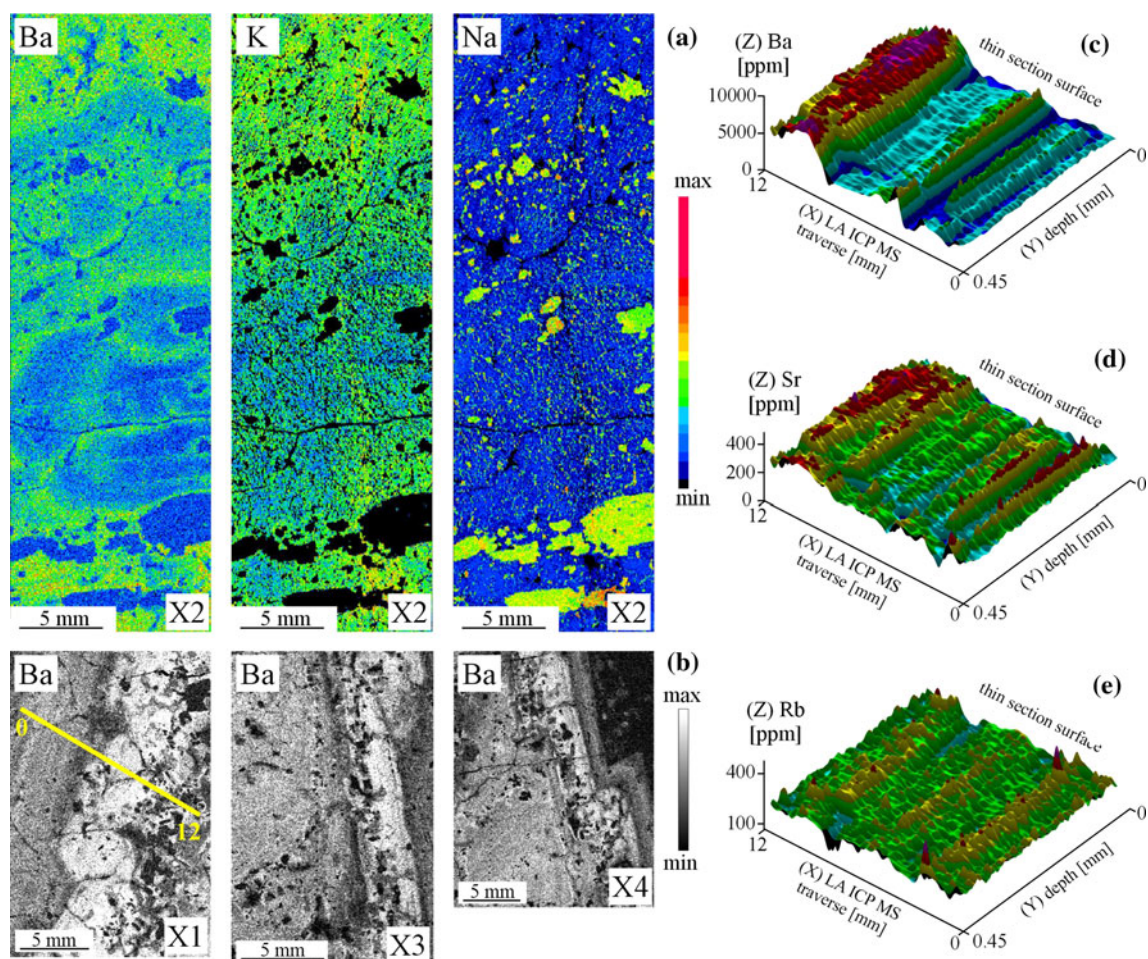


Fig. 5 Composition of porphyritic granite megacryst X. **a** Evidence for syneusis in Ba thin-section maps (X2). **b** Ba-distribution maps show the feldspar margin in slices X1, X3 and X4 (left to right). Though all the patterns of the Ba-rich zone are different, all demonstrate very dynamic process of barium incorporation; **c,d,e** 3D depictions of Ba, Sr and Rb distribution (along yellow

transect on thin-section map) in X1 (further patterns in Electronic Supplement Fig. 3). In contrast to sample RQ and B1 (Figs. 3, 4), all the X patterns (Ba, Sr, Rb) are dissimilar and display the highest complexity in trace-element distribution. *Yellow line*—LA-ICP-MS transect. Crystal margin (left) and crystal core (right). Axes X, Y and Z are as in Fig. 3

and to what extent the relationship is accordant, non-accordant, or random. The initial stage in the analytical process is shown in Fig. 6.

Large differences characterize the concentrations of the selected elements. Thus, using absolute values in the model is unlikely to give results (Fig. 6) useful to the tracking of differences in element behavior during crystallization.

Normalization is required and was accomplished as follows. For each analyzed traverse and element set, the concentration value (in ppm) separating each local minimum from the adjacent maximum was designated the “cut-off value” (Fig. 7). In most cases, the cut-off value matched the average value of each element over the total area analyzed. Only in some cases was the cut-off value adjusted (by <10% of the average) so as to include a local maximum or minimum concentration value. The entire population of data was then viewed as a binary system.

After setting the cut-off value for each element in the analyzed crystal, distribution patterns can be compared in two ways: ‘probabilistic’—based directly on the data collected by LA-ICP-MS or ‘non-probabilistic’—based on interpolated distribution models. Both of these approaches have their advantages and drawbacks. The ‘probabilistic’ approach can introduce measurement errors into the model and is free of uncertainties caused by interpolation. Though these features make the ‘probabilistic’ approach more reliable, this approach does not fully encompass the spatial relationships of the data as only data from discrete collection points is involved in the comparison. In the ‘non-probabilistic’ procedure, absolute values of an element concentration are used to interpolate distribution models that show clear zoned texture. Interpolation allows reconstruction of the shape of the isoline of an element concentration equal to the cut-off level. The drawback in this

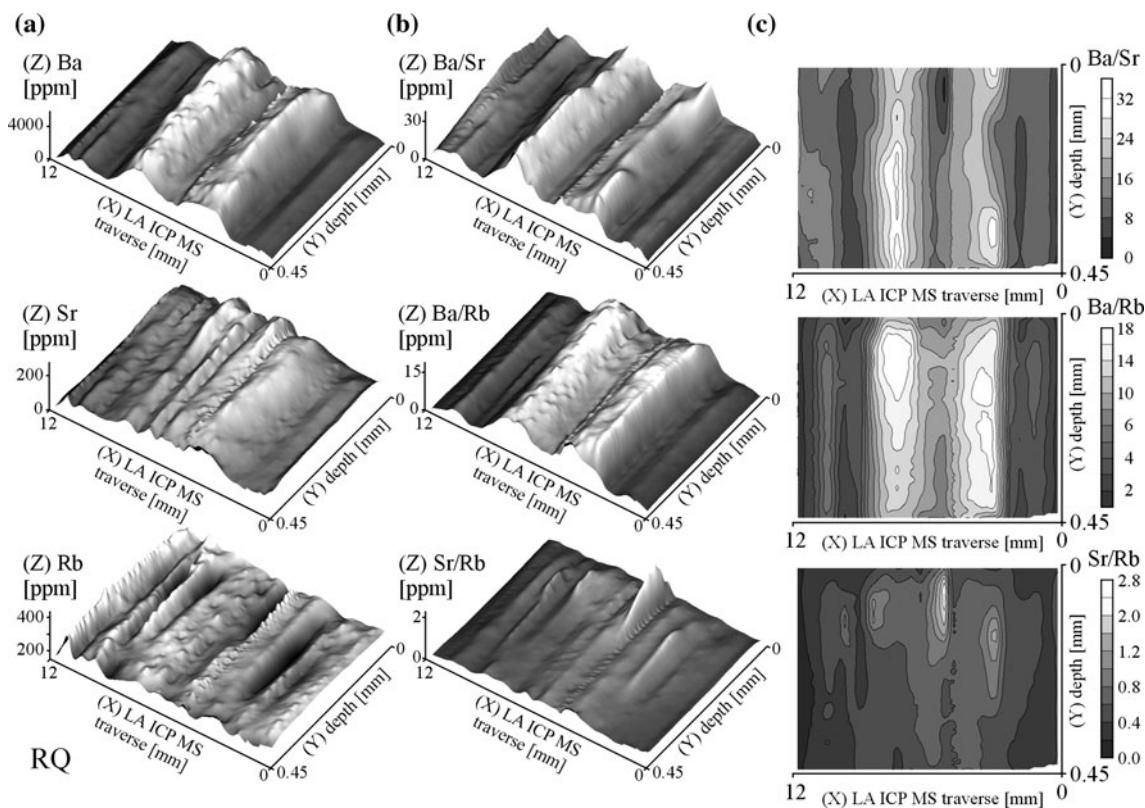


Fig. 6 Trace-element distributions and their mutual relations—based on absolute concentration values for feldspar RQ. Strontium distribution is a weak reflection of that of barium, whereas rubidium displays an entirely different pattern. None of the patterns correlate well with the compositions of coherent and active magma domains (whole rock composition). Positive linear correlation between Ba and

Sr in mixed magmas and negative correlation with Rb is not reflected in the spatial distribution of these trace elements in the crystal. As barium predominates over both other elements, Ba/Sr and Ba/Rb patterns are similar to barium alone and do not allow easy evaluation of any behavioral differences: Axes X, Y and Z are as in Fig. 3

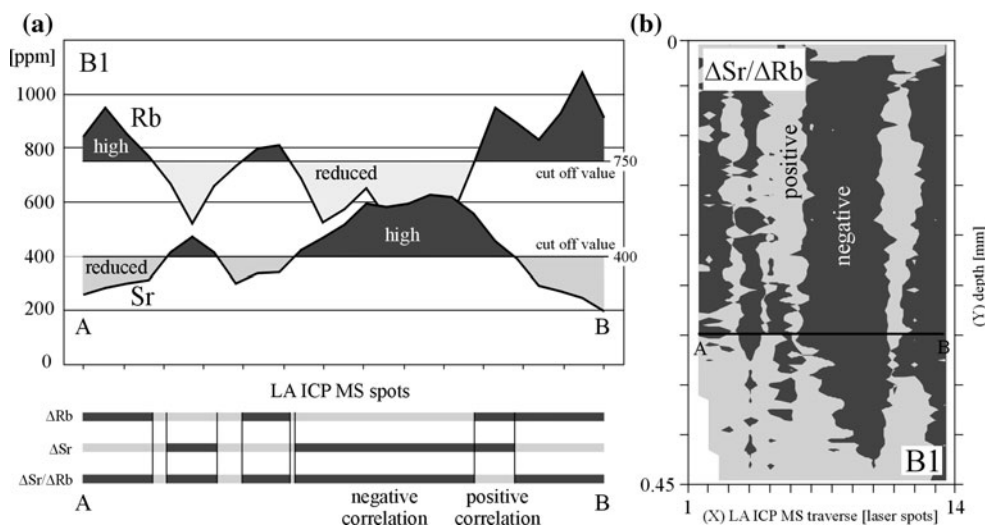


Fig. 7 **a** The ‘non-probabilistic’ method used to determine the degree of accordance between two element contents presented on the single cross-section through the concentration distribution model (Rb and Sr in feldspar B1). The ‘cut-off value’ separating ‘high’ and ‘reduced’ element contents is 760 ppm for Rb and 400 ppm for Sr. The Rb and Sr bars in the lower part of the diagram show areas of

high (dark gray) and reduced (light gray) values. The lowest Sr/Rb bar showing regions of ‘positive’ and ‘negative’ correlation constitutes the input data for the single line of the output concentration model. **b** The distribution of ‘positively’ and ‘negatively’ correlated values for Sr and Rb in feldspar B1. Axes: X—LA-ICP-MS spots along traverse, Y—depth of analysis (mm)

Table 2 ‘Probabilistic’ (quaternary and binary variation) and ‘non-probabilistic’ (binary variation) models showing the degree of accordance in element behavior during the crystallization process based on relative values of element content (cut-off models)

Sample	Cut-off ‘probabilistic’ model					Cut-off ‘non-probabilistic’ model			
	Quaternary variation				Unc. area (%)	In the certainty area		Positive (%)	Negative (%)
	Positive		Negative			Positive (%)	Negative (%)		
	+/+ (%)	-/- (%)	+/- (%)	-/+ (%)	Positive (%)	Negative (%)	Positive (%)	Negative (%)	
<i>ΔBa/ΔSr</i>									
B1	23.1	45.7	1.8	10.1	19.3	85.4	14.6	83.4	16.6
RQ	33.0	46.0	1.1	1.6	18.3	96.7	3.3	92.6	7.4
X1	25.1	35.5	5.5	5.7	28.2	84.6	15.4	74.1	25.9
X2	26.1	28.7	6.4	7.0	31.8	80.8	19.2	72.5	27.5
X3	49.7	18.8	4.6	1.2	25.7	92.3	7.7	85.6	14.4
X4	32.9	19.3	3.1	0.4	44.3	94.0	6.0	75.6	24.2
<i>ΔBa/ΔRb</i>									
B1	10.6	28.2	6.8	23.7	30.7	56.1	43.9	53.7	46.3
RQ	13.7	18.7	20.9	23.6	23.1	42.2	57.8	43.9	56.1
X1	14.1	15.8	10.8	13.0	46.3	56.4	43.6	50.4	49.6
X2	7.8	24.8	17.5	5.2	44.7	59.7	40.3	55.0	45.0
X3	6.7	4.9	30.6	9.2	48.6	23.4	76.6	25.6	74.4
X4	11.9	4.2	19.6	10.5	53.8	36.8	63.2	36.7	63.3
<i>ΔSr/ΔRb</i>									
B1	12.3	21.0	12.0	16.3	38.4	54.8	45.2	47.8	52.2
RQ	13.2	17.6	23.8	21.1	24.3	41.0	59.0	42.2	57.8
X1	11.2	12.2	8.7	15.3	52.7	50.4	49.6	46.6	53.4
X2	7.4	14.4	18.2	6.2	53.8	48.6	51.4	45.3	54.7
X3	4.2	6.9	24.9	9.6	54.4	26.5	73.5	27.1	72.9
X4	6.2	3.9	20.7	13.4	55.8	24.9	75.1	28.6	71.4

The degree of accordance in element behavior is expressed as a percentage. Positively correlated and negatively correlated regions in the various elemental depictions are shown in Fig. 8, in Electronic Supplement Figs. 3 and 4 and explained in Fig. 7

unc uncertainty

case is that measurement errors are not introduced. Both of these approaches were used and the results compared.

In the ‘probabilistic’ approach for the Ba, Sr, and Rb concentration data, probabilities for four possible variations between any two of the elements were separately calculated. The four possibilities were (1) both elements relatively increased, (2) both reduced, (3) element A increased and B reduced, and (4) element A reduced and B increased. The base for comparison was their cut-off values in all cases (Table 2). The results can be reduced to two possibilities—(1) and (2) were deemed positive correlations between relative values and (3) and (4) as negative correlations. All calculations involved error in the measurements taken by LA-ICP-MS and normal distribution of the error. Where one or both of the compared concentration values were close to their cut-off value, measurement error will have led to uncertainty of the increased/reduced estimation. As the resulting probability of the estimation of positive/negative correlation was low, the related spot

measurement was deleted from the database (Table 2). We used >85% or <15% probability as a divider (<15% probability of positive correlation is equivalent to >85% of a negative correlation). We calculated a ratio of correlation between the distributions of elements based only on data of high certainty (Table 2). This approach enabled plots of relations between probability of correlation, two-element relative values and absolute values in ppm of either to be created (see Electronic Supplement Fig. 2).

In the ‘non-probabilistic’ approach, all concentration values above the cut-off level were simply deemed ‘high’ and given a value of 1, and a dark color on the interpolated model (Fig. 8). All values below the cut-off level were deemed “reduced” and given a value of -1, and a light color on Fig. 7. The element distributions recast in this way enable the degree of spatial accordance or non-accordance between two element contents (e.g., Rb and Sr) to be examined further (Fig. 7). In the output model, a value of 1 (‘positive correlation’ on Fig. 7) indicates spatial

accordance of “high” or “reduced” values (ΔRb and ΔSr) for the two elements ($1/1 = 1$ and $-1/-1 = 1$). A value of -1 (‘negative correlation’ on Fig. 7) corresponds to non-accordance, i.e., a high value in the concentration of one element spatially linked to a low value of the second ($1/-1 = -1$ and $-1/1 = -1$). Although the error of the measurements is not introduced (and interpolation itself is causing uncertainty), areas of possible mismatch are limited to those close to the cut-off isoline on either of the compared models.

In both approaches, the percentages of “positively” and “negatively” correlated values describe the mutual behavior of element pairs in the crystal section. Values close to 100, 0, and 50% indicate full accordance, total non-accordance, and lack of any correlation, respectively.

The degree of accordance or non-accordance in element behavior during advection–diffusion as deduced from both ‘probabilistic’ and ‘non-probabilistic’ output models is summarized in Table 2. Maps showing element distributions above and below the “cut-off value” for feldspars RQ, B1 and X1–X4 (upper row) and corresponding ‘non-probabilistic’ output models of their correlation (lower

row) are shown in Fig. 8 and in the electronic supplement (Figs. 3, 4).

In the mixed magmas, Ba and Sr strongly correlate. Neither shows any strong correlation with Rb. All of the concentration output models confirm the similar behavior of Ba and Sr in feldspar domains. The degree of accordance for $\Delta Ba/\Delta Sr$ is always high. In the “non-probabilistic” model, two sections of feldspar X (3–4) show complementary “positively” to “negatively” correlated values for $\Delta Ba/\Delta Sr$ with $\Delta Ba/\Delta Rb$ and $\Delta Sr/\Delta Rb$ (Fig. 8). The high positive correlation level of $\Delta Ba/\Delta Sr$ for the remaining samples contrasts with the lack of such correlation between $\Delta Sr/\Delta Rb$ and $\Delta Ba/\Delta Rb$ (see Supplement Figs. 3, 4).

The quaternary variation (“probabilistic model”) carries different chemical implications for each feldspar type and can be more precisely correlated with a particular stage of mixing between two magmas than can the binary variation (Table 2). By differentiating between these stages in the mathematical model, it is possible to discriminate periods of growth in each coherent/active environment thereby providing a more complete record of mineral residence and

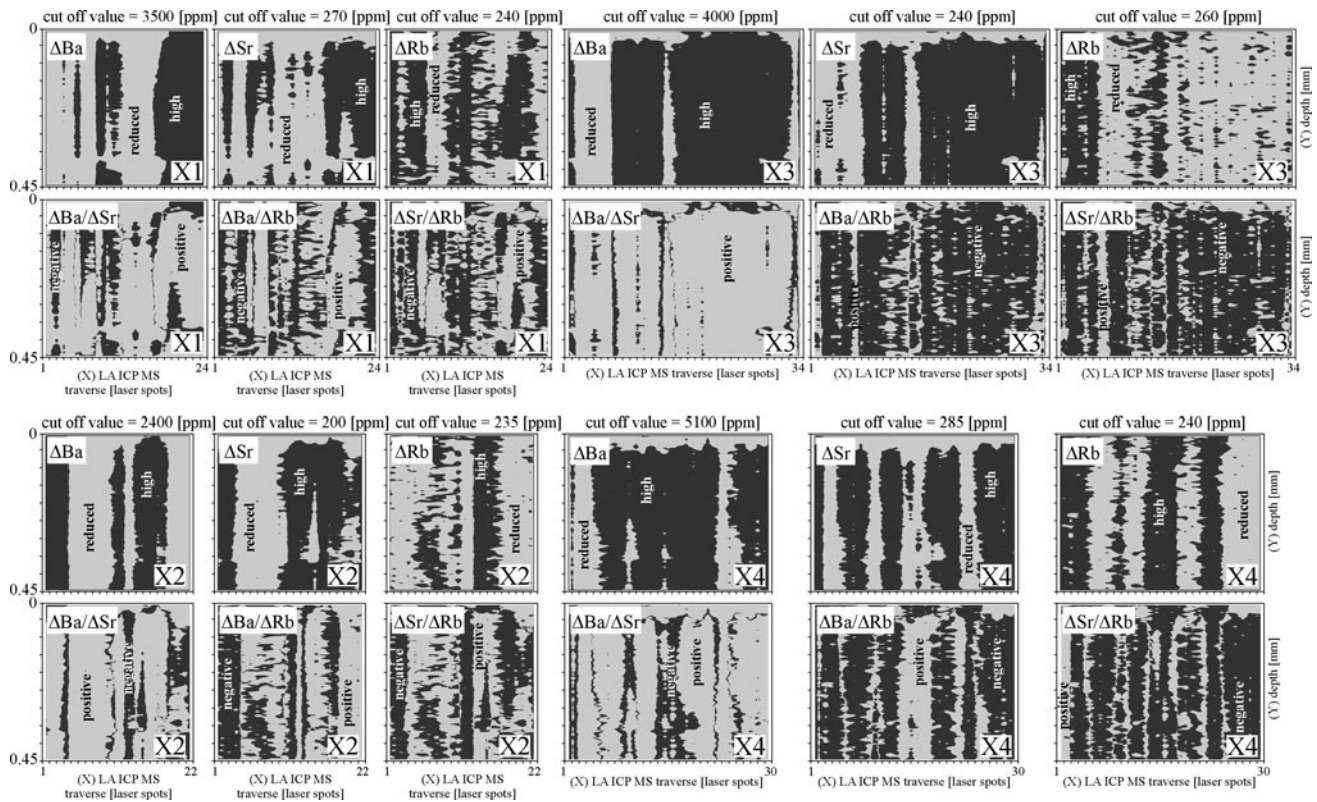


Fig. 8 Spatial elemental distributions (ΔBa , ΔSr , ΔRb) for feldspar X (see Electronic Supplement Figs. 3, 4 for RQ and B1) generated by using “cut-off values” and output concentration ‘non-probabilistic’ models illustrating the degree of accordance between two elements. The ‘cut-off values’, the basis for splitting the depictions into dark

and light parts, is given above each. Axes: X—LA-ICP-MS spots along traverse, Y—number of laser impulses, i.e., depth and duration of analysis (1 s to 5 μm). Proportions of light and dark areas are given in Table 1

growth. The $\Delta\text{Ba}/\Delta\text{Sr}$ ratio marked as ‘+/+’ and ‘-/-’ point to crystallization in magma domains enriched in mafic and granitic components, respectively. Both ‘+/-’ and ‘-/+’ variations are low.

Crystal domains with values of $\Delta\text{Ba}/\Delta\text{Rb}$ and $\Delta\text{Sr}/\Delta\text{Rb}$ marked “+/-” versus “-/+” are related to crystallization in active magma regions enriched in mafic or granitic components, respectively. Domains marked as ‘-/-’ reveal a tendency toward magma homogenization—growth in well-mixed intermediate magma. A positive ‘+/+’ correlation reflects intermediate concentrations, in mixed magma, where the trace elements derived from both mafic and granitic end members are enriched in feldspars. This condition is difficult to explain, but one possible explanation is that residence in a heterogeneous mafic magma dominated region with Rb enrichment involved accelerated diffusion and, simultaneously, delayed Sr migration. Hence, co-enrichment may not be an equilibrium process in this case. This ‘+/+’ covariation may result from resorptive recrystallization during transit through mafic mixed magma.

Element behavior during crystallization: gradient models

The next aim was to develop a more precise way of showing the degree to which the behavior of two elements persisted during the same process. As the feldspar grew in magmas of different compositions, the absolute values of two elements should rise and fall simultaneously during the process if the two are correlated. The degree of continuity in the behavior of each element (the concentration gradient) in a direction parallel to that of crystal growth was determined using the first derivative. For every analyzed transect (Figs. 3, 4, 5), the rate and direction of change in element concentration was calculated. Again, a ‘probabilistic’ approach based directly on LA-ICP-MS data and a ‘non-probabilistic’ approach based on interpolated models of element content were used (Table 3; Fig. 9; Supplement Figs. 5, 6, 7).

In the ‘probabilistic’ approach, the gradient was calculated using absolute values of the same element measured by LA-ICP-MS from the same depth in two adjacent spots. If the difference between the two absolute concentration values is less than 4.6% of the value of the greater of the two, it follows that the probability of the correct estimation of the gradient is less than the probability inside the σ range of the normal distribution due to the 7% sigma error of the measurement. All such situations were deemed uncertain and the data involved ruled out of further calculations of gradient correlation. From the remaining data, correlations between gradients of every pair of elements were calculated.

In the ‘non-probabilistic’ approach, gradient values were calculated for the interpolated distribution models. The models were normalized to 1 or -1 (increase or decrease in element concentration). As before (see Fig. 7), dividing the models of normalized gradient for two different elements on the same transect leads to an output model quantifying the match or contrast in gradients (Electronic Supplement Fig. 5). In this gradient output model, positive values correspond to zones where the concentrations of two elements simultaneously increase or decrease, negative values to zones where an increase in the concentration of one is associated with a decrease in that of the other.

In both approaches, percentage values of positive and negative correlations for the analyzed data set were calculated. Values approaching 100% indicate a strong accordance, values close to 0%, complete discordance and values $\sim 50\%$, no preferred pattern of behavior.

The degrees of accordance in gradient increase or decrease for X, and for both other crystals, are given in Table 3. These show further clear trends in element behavior. The match of Ba and Sr is again obvious. Compared to the concentration models, the degree of dBa/dSr accordance is lower in the gradient models. The dBa/dRb and dSr/dRb values for feldspar X sections (3–4) do not match the concentration model values; they show almost no correlation. In addition, for all of the feldspars, both of these derivative ratios show a clear tendency to oscillate around 50%, i.e., to show no preferred pattern.

The output models are shown in Fig. 9 and in Electronic Supplement Figs. 6 and 7. They demonstrate complicated patterns reflecting local changes in element gradients in magma domains advected to growing crystal surface. Crystal X exhibits the greatest degree of complexity in magmatic field composition during its growth. For all sections of this crystal, the gradient models and their correlations are shown in Fig. 9.

Discussion

Heterogeneity in magma domains, and differences in the rate of element fractionation between domains, is considered to have been the main reason for the observed complexity in the spatial distribution of elements in the feldspar crystals. Detailed studies of Karkonosze crystal geochemistry provide various lines of evidence for this view (Słaby et al. 2007a, b, 2008a, b). Any interpretation of detected element variability within the crystals requires certainty that the variability is a primary feature inherited from the igneous system. Every secondary process needs to be ruled out. A possibility exists, for instance, that the complexity may have been enhanced by differences in the diffusivities of the different elements within the crystals. Diffusivity is

Table 3 ‘Probabilistic’ and ‘non-probabilistic’ models showing the degree of accordance in element behavior during the crystallization process based on gradient of element content (gradient models)

Sample	Gradient ‘probabilistic’ model				Gradient ‘non-probabilistic’ model		
	Positive (%)	Negative (%)	Uncertainty	In the certainty area		Positive (%)	Negative (%)
				Positive (%)	Negative (%)		
<i>dBa/dSr</i>							
B1	55.6	24.9	19.5	69.1	30.9	66.2	33.8
RQ	73.2	9.0	17.8	89.1	10.9	83.6	16.4
X1	47.7	26.5	25.8	64.3	35.7	58.0	42.0
X2	59.1	18.6	22.3	76.1	23.9	69.1	30.9
X3	56.8	16.8	26.4	77.1	22.9	70.1	29.9
X4	65.6	7.1	27.3	90.2	9.8	81.7	18.3
<i>dBa/dRb</i>							
B1	56.7	25.9	17.4	68.6	31.4	61.7	38.3
RQ	45.8	34.4	19.7	57.1	42.9	46.8	53.2
X1	49.1	22.4	28.5	68.7	31.3	70.0	30.0
X2	36.1	35.7	28.1	50.3	49.7	49.3	50.7
X3	38.1	28.3	33.6	57.4	42.6	53.7	46.3
X4	31.6	29.7	38.7	51.5	48.5	47.5	52.5
<i>dSr/dRb</i>							
B1	48.3	28.2	23.5	63.1	36.9	52.5	47.5
RQ	40.2	39.4	20.4	50.5	49.5	39.0	61.0
X1	40.1	27.7	32.2	59.2	40.8	53.0	47.0
X2	35.1	28.2	36.7	55.5	44.5	47.0	53.0
X3	30.4	34.9	34.7	46.5	53.5	46.9	53.1
X4	27.2	39.4	33.4	40.8	59.2	40.8	59.2
In the certainty area				Uncertainty (%)		Amount of data	
<i>PIP/P</i> (%)		<i>PIP/N</i> (%)		<i>NIP/P</i> (%)		<i>P/NIP</i> (%)	
<i>dBa/dSr/dRb</i>							
B1	52.6	17.9	10.9	18.7	28.4	2,226	
RQ	49.2	39.4	3.4	8.0	26.4	1,253	
X1	46.3	17.8	13.0	22.9	39.0	2,146	
X2	40.1	34.7	14.4	10.9	40.9	1,970	
X3	40.0	37.5	6.7	15.9	43.2	3,053	
X4	42.2	47.3	2.4	8.1	45.1	2,694	

The degree of accordance of element behavior is expressed as a percentage. For depictions, see Fig. 9 and Electronic Supplement Figs. 6 and 7. Acronyms: *PIP/P*—common behavior of all elements; *PIP/N*—only Ba and Sr accordant; *NIP/P*—only Sr and Rb accordant; *P/NIP*—only Ba and Rb accordant

determined, inter alia, by the density of crystal defects, related in turn to the quantities and types of dopants present.

Incorporation of Ba into feldspars causes local structural distortions due to coupled KSi–BaAl exchange (Viswanathan and Brandt 1980; Viswanathan and Kielhorn 1983). This distortion leads to an increase in Al–O[−]–Al defects (Marfunin and Bershov 1970; Słaby et al. 2008a). Though the highest Ba contents occur in B1, X3, and X4, the same feldspar samples also show lower Rb mobility (low

$\Delta\text{Ba}/\Delta\text{Rb}$) than do the remainder (Table 2, non-probabilistic model—area of certainty). The Al–O[−]–Al defects exert no obvious influence on any diffusing Rb. In addition, the gradient models show that local Ba/Rb arrangement does not differ significantly from that in the other samples. However, lower Rb mobility is clear in both models for B1 and X4.

Combined trace-element and cathodoluminescence studies have shown the probable influence of water species on the defect distribution pattern (Słaby et al. 2009). The

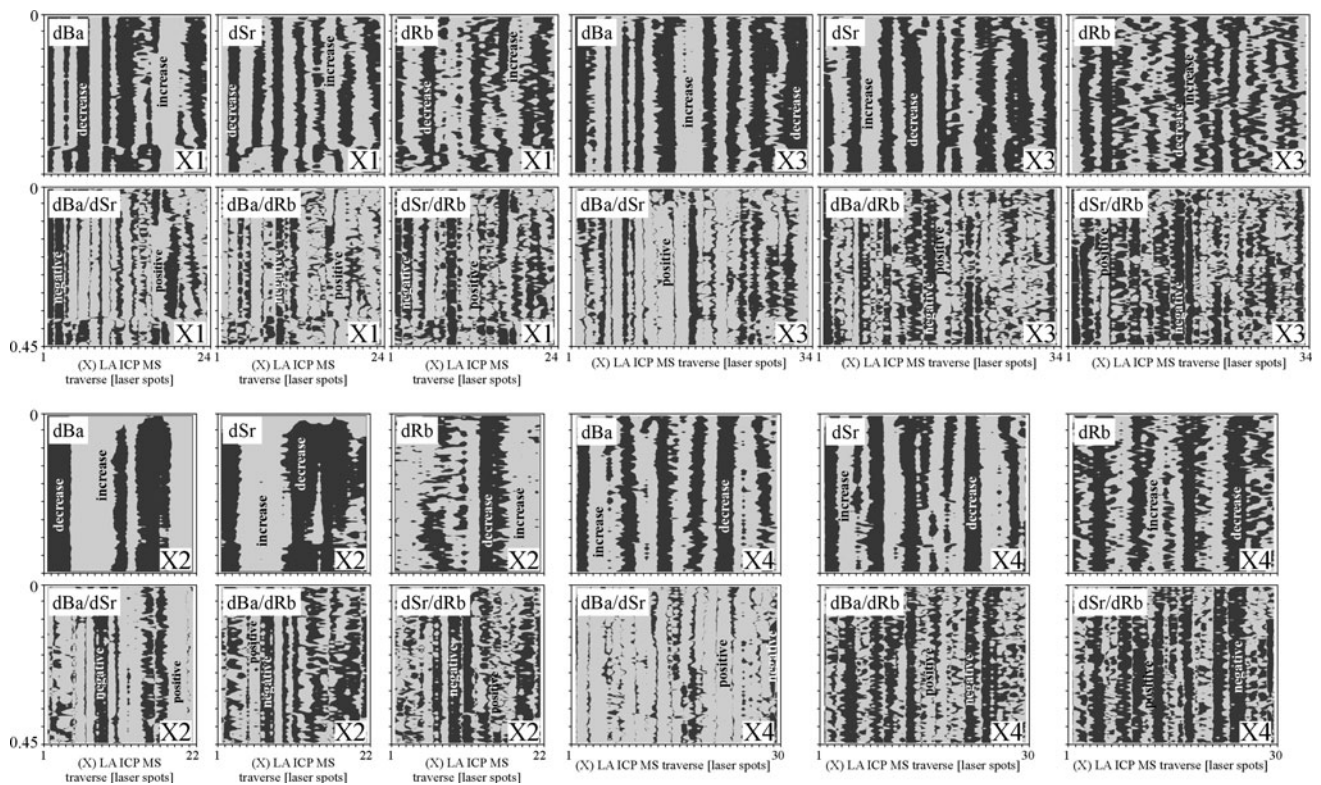


Fig. 9 The gradient directions (dBa, dSr, dRb) of changes in trace-element concentrations (*upper row*) in feldspar X (see Electronic Supplement Figs. 6, 7 for RQ and B1) and output gradient models (*lower row*) showing the degree of accordance between gradients of element pairs. As explained (see Electronic Supplement Fig. 5), *light-gray regions* reflect accordance of element behavior and *dark-gray*

regions, discordance; proportions are given in Table 2. Note differences with the output models presented on Fig. 8. The more sensitive gradient model provides a more detailed picture of local conditions during element incorporation into the growing crystal. Axes: X—LA-ICP-MS spots along traverse, Y—number of laser impulses, i.e., depth and duration of analysis (1 s to 5 μm)

feldspars, nominally anhydrous, carry significant if variable amounts of water. Water heals and rearranges the Al–O[−]–Al defects (Finch and Klein 1999; Graham and Elphick 1990, 1991; Słaby et al. 2009). However, water also commonly promotes hydroxyl defects (Kronenberg et al. 1996) that trigger further significant redistributions among sites, thus increasing diffusion. Water also substitutes for potassium occupying sites also favored by rubidium (Kronenberg et al. 1996). As the feldspars crystallized from magmas variably saturated in volatiles, it would be no surprise if water influenced element diffusion between magma domains and also in the crystals after initial element incorporation. However, even though the amount of water is relatively high in the late hybrids represented by B1, the sample is characterized by lower rubidium mobility. The fact that the level of water present at which diffusion is most efficient in feldspars is not yet known is pertinent here.

Small amounts of impurities (trace-element dopants) can control diffusion rates in silicates and offset the effect of water. As with the potential role of water, their contribution to the abundance of other defects is difficult to predict.

Their different positions in the feldspar structure can result in one impurity largely compensating for the effects of another (Kronenberg et al. 1996; Petrov 2002). Kronenberg et al. (1996) point to complexity in the multivalent dopant and hydroxyl defects relationship in local charge balance accommodation, and Petrov (2002) emphasizes the role of dopants in feldspar structure distortion. Potential influences on diffusivity are clearly multi-faceted.

Any effect of dopants on inter-crystal diffusion of Ba, Sr, and Rb seems to be negligible at best. Cherniak (1996, 2002) showed that in an alkali feldspar crystal, Ba diffusion is slower than that of Sr by about two orders of magnitude. Giletti (1991) experimentally determined that the activation energy for Rb was higher than that for Sr. Thus, the Ba and Sr patterns in the Karkonosze crystals would likely have been stable for a long time under extreme thermal conditions $\sim 700^\circ\text{C}$ in the case of the Karkonosze pluton; the predictions of Cherniak (2002) are 10^9 and 10^7 , respectively. The pluton formed within the time span 328 ± 12 to 302 ± 6 Ma (Kusiak et al. 2008; Mikulski and Stein 2007). Late-stage hydrothermal activity at $<500^\circ\text{C}$, at which diffusion would have been inefficient, is dated at

294 Ma (Mikulski et al. 2004). Thus, on balance, the earliest space distribution pattern of the three investigated elements is unlikely to have been changed significantly due to intra-crystal diffusion. Consequently, one may assume that the conceptual models demonstrate element behavior reflecting their variable mobility in an open igneous system.

Being definitive about element behavior in an open magmatic system is difficult because of the significant number of variables involved. Experiments that embrace only some of these provide a simpler and more easily controlled system. The feldspars examined here are the products of the mixing of two end-member magmas, one granitic, one mafic, each evolving in its own independent reservoir (Słaby and Martin 2008). The evolution in both reservoirs was driven by fractional crystallization. At intervals during this process, communication between the reservoirs led to mafic magma entering the granitic magma chamber where mixing occurred. Late mafic dykes show that mantle-derived magma of distinctly different composition was also directly injected into the granitic chamber without passing through the mafic chamber. Even if all mixing occurred between the two fractionating magmas, their compositions cannot now be precisely determined. The whole system is characterized by extreme heterogeneity.

In addition, fluids of mixed (mantle-crust) origin interacted with the pluton at a late stage in its evolution (Kusiak et al. 2009; Słaby 2005; Słaby et al. 2005). Water changes rheological properties, among others, ionic diffusion rates (e.g., Holloway 1987; Hirschmann 2006; Kohlstedt et al. 2000). However, the whole rock Ba-Sr-Rb geochemical signature appears to have been controlled mainly by mixing (Słaby et al. 2008a).

A question arises. Do the conceptual models truly reflect the system heterogeneity? The macroscale reflected in whole rock composition and the microscale reproduced in the conceptual models clearly differ. Whole rock composition shows strong positive correlation between Ba and Sr and negative correlation of both with Rb. In contrast, all of the models show strong correlation between Ba and Sr and almost none between either of them and Rb. Correlation, or the lack of it, may reflect different element mobilities (diffusivities) during the mixing process or differences in element compatibility with a crystallizing solid. A recent simulation by Perugini et al. (2008) is of particular importance for studies of single-phase heterogeneity such as the present one. Their experiment demonstrated that mixing does not show linear trace-element behavior during exchange on a short time span.

The growth morphologies and compositions of the feldspars mirrored in the models indicate that crystallization continued as they migrated through a heterogeneous magmatic field. Felsic magma domains were relatively Rb-

rich and Ba- and Sr-poor and mafic domains, the reverse. If the feldspars had migrated between two coherent domains only, alternate compositional zones should reflect migration from one to the other. In such a case, in all of the output models (Tables 2, 3), the positive values of $\Delta\text{Ba}/\Delta\text{Sr}$ and $d\text{Ba}/d\text{Sr}$ should tend to 100% as should negative values of $\Delta\text{Ba}/\Delta\text{Rb}$ and $d\text{Ba}/d\text{Rb}$, and values of $\Delta\text{Sr}/\Delta\text{Rb}$ and $d\text{Sr}/d\text{Rb}$. The “probabilistic” and “non-probabilistic” models show that no one of the magma domains represents an entirely coherent composition. They are all hybrid, active domains. Barium and strontium are strongly correlated in all—in a particular area in ‘probabilistic’ models (Table 2) and as a more widely developed positive correlation in ‘non-probabilistic’ models (Table 3). The degrees to which Ba and Sr each behave differently to Rb vary, but in both cases, mostly oscillate around 50% (Tables 2, 3); a lack of any correlation is indicated. The positive and negative $\Delta\text{Ba}/\Delta\text{Rb}$ values on Table 2 (“non-probabilistic” model) show no systematic bias favoring one or the other. In contrast, a persistent tendency for negative $\Delta\text{Sr}/\Delta\text{Rb}$ values to be higher suggests that the faster-moving element is Rb.

The heterogeneous nature of the magma domains advected to the growing crystal surfaces is more apparent in the “probabilistic” models using quaternary variation. These models differentiate more precisely between the domains and allow division into four groups. Variable proportions between the four groups indicate a continuous process of hybridization. The magmatic field seems to be composed of variably mixed domains strongly enriched in mafic- or felsic components (+/+ and -/- for $\Delta\text{Ba}/\Delta\text{Sr}$; +/- and -/+ for $\Delta\text{Ba}/\Delta\text{Rb}$ or $\Delta\text{Sr}/\Delta\text{Rb}$; Table 2) with some tending to homogenization (+/- for $\Delta\text{Ba}/\Delta\text{Sr}$; -/- for $\Delta\text{Ba}/\Delta\text{Rb}$ or $\Delta\text{Sr}/\Delta\text{Rb}$; Table 2). There are also some domains marked as +/+ for $\Delta\text{Ba}/\Delta\text{Rb}$ or $\Delta\text{Sr}/\Delta\text{Rb}$ (Table 2) which may indicate feldspar recrystallization after partial remelting. However, strong Ba vs. Sr correlation, and coupling with LREE, in many such domains argue against it (Słaby et al. 2008a).

The models clearly suggest a heterogeneous growth environment, but do they suggest that different advection/diffusion rates applied during feldspar crystallization? As Rb migrated between domains, it left Ba and Sr behind; Ba and Sr, are strongly correlated, whereas Rb is not correlated with either. The fact that value of correlation calculated within certainty areas in “probabilistic” models is similar to those with correlation level close to 50% in “non-probabilistic” models argues against random measurement error and in favor of proper interpolation and real lack of correlation between Ba/Rb and Sr/Rb. Is the lack of correlation evidence for fast Rb diffusion? One might relate large areas of uncertainty in the cut-off value models to fast Rb diffusion which would compensate for local

concentration. Thereby, the ability to test the diffusivity accurately is lost.

The quaternary variation correlations between Ba and Sr also show some rules. The more they tend toward coherent magma composition (+/+, -/-), the larger the certainty area appears in the models. The best correlations for $\Delta\text{Ba}/\Delta\text{Sr}$ are evident for B1, RQ, and X3. At the same time, they demonstrate the smallest dead-zone uncertainty. The uncertainty grows as the element concentrations approach the cut-off value, i.e., mixing proceeds toward blending (Table 2; Electronic Supplement Fig. 2). This tendency is poorly visible for Ba/Sr, much better for Sr/Rb and Ba/Rb. Rubidium should approach the cut-off level first due to the small difference in its concentration in both end-member magmas and due to its diffusivity being the greatest of all three. Consequently, the models should reveal the largest areas of uncertainty for Ba/Rb and Sr/Rb pairs. Assuming that Sr diffuses a little bit faster than Ba, the uncertainty area for $\Delta\text{Sr}/\Delta\text{Rb}$ should be bigger than that for $\Delta\text{Ba}/\Delta\text{Rb}$. In all cases, for both types of models, and all feldspars, this is the case. This may be an argument for the differences recognized in diffusion rates recognized by the models. It may also serve as an example of the microscale experimental reproducibility in the solid phase reported by Perugini et al. (2008). The argument is not strong as all of the investigated elements are compatible. They may be fractionated by a chemical potential gradient such as differences in compatibility with a crystallizing solid, their diffusion controlled mainly by valence and interaction with tetrahedral Al in the melt (e.g., Acosta-Vigil et al. 2006; Morgan et al. 2008; Acosta-Vigil et al. 2005).

The role of compatibility in element fractionation is apparent in the gradient models, where all considered pairs of the three elements show preferences toward positive correlations (Table 3; *P/P/P* values). As with the cut-off value models, the gradient models show a clear relationship between Ba and Sr. However, any Rb anti-correlation is barely evident. By dividing the data into populations below and above a cut-off value, the “non-probabilistic” concentration model reveals a more general tendency. The quaternary variation enables a more precise recognition of magmatic field heterogeneity. The gradient model, by taking into account local gradient changes, is more sensitive to every change and provides a more detailed picture of chaotic element behavior during incorporation into the growing crystal. Due to this, the areas of certainty and uncertainty differ significantly, the latter being considerably reduced.

The gradient output models for RQ and X4 provide clear evidence of crystallization proceeding in active magma domains with compositions locally very much enriched in mafic components. Barium and strontium are strongly positively correlated. Some anti-correlation with rubidium

is evident (Table 3, compare *P/P/N* and *P/N/P* areas). Less clear trends, though still consistent with that observed for RQ-X4, are also evident for X2-3 (Table 3). In the remaining samples, rubidium correlation with barium is stronger than any for strontium. The explanation may reflect differences in the magmas during mixing or during chamber replenishment; the RQ feldspar grew from a hybrid belonging to an early mixing stage and B1 and X1-4 from a hybrid with a late-mixing signature. The behavior of X4 tells of an early hybrid, whereas the active magma domain is typically preserved in feldspars crystallized from a late hybrid. Early hybrids preserve the more pristine end-member magma compositions more completely, whereas late hybrids derived from already fractionated and mixed magmas do not. In Karkonosze, fractionation of both magmas resulted in their depletion in Ba and Sr and enrichment in Rb, but the level of change in each was different. In the felsic magmas, the general partition coefficient for Ba, Sr, and Rb is $D = \sim 10, \sim 9, >1$ (Słaby and Martin 2008). In the mafic magmas, Sr is exhausted more efficiently (plagioclase fractionation) than Ba and Rb, changing proportions between them at all stages of differentiation. Preferences in compatibility with a crystallizing solid can explain their behavior; incorporation was controlled mainly by valence and melt composition, especially Al_2O_3 content (Ren 2004).

Another explanation is also possible. Whole rock composition synthesizing the temporal and chemical evolution of Karkonosze granitic magma indicates at least three stages of replenishment, each involving different end-member magma compositions (Słaby and Martin 2008). A hybridic rock sequence implies a long-lived mafic magma source coexisting with a granitic chamber and argues for a deep-seated mafic magma chamber rather than for continuous mantle melting. The microscale feldspar models indicate that at the last stage of pluton evolution fractionated and not fractionated (pristine) mafic magma was supplied. This means that mafic magma was supplied via mafic chamber as well as via direct injection into the granitic chamber without passing through the mafic chamber.

Feldspar X provides the most informative data about the complexity of the active and coherent domain patterns within the heterogeneous magmatic field (Figs. 8, 9). Element mobility between magma domains for feldspars B1 and RQ was retrieved on the basis of one transect in each case. The four X feldspar slices present four very different images of the magma mixing field in which feldspar growth occurred. The concentration patterns show (cut-off value models) that the feldspar migrated in a field of domains ranging from near-coherent to active. The gradient models demonstrate that change in a local environment, supposedly involving a coherent magma domain, actually

involved active subdomains. Further, the patterns of the active domains denote compositional variety, heterogeneity, and complicated chemistries. The heterogeneity is due to chaotic mixing proceeding hand-in-hand with the fractionation of elements during crystallization. Though every sector of crystal X differs in composition, both models show that the growth of all was governed mainly by a single process. That process delivered elements in differing proportions to the growing crystal surface as mixing and chemical exchange continued. As with feldspars RQ and B1, no single inter-element relation in any of the feldspar X models is linear. In addition, the gradient models for feldspar X reveal a detailed, local pattern that points almost exclusively to growth in active magma domains with significant exchange of Sr and Rb and delayed, yet mobile, Ba.

Conclusion

New models provide a tool for tracking, on a microscale and at two levels of precision, geochemical heterogeneity in growing crystals. At both levels, the characteristics of a chaotic system are evident. Concentration models and gradient models reveal similar patterns of accordance–discordance in element behavior, though the latter provide a more detailed level of information.

Both gradient and concentration models confirm the experimental results and conclusions of Bindeman and Davis (1999), De Campos et al. (2004, 2008, 2010), García-Moreno et al. (2006), Kouchi and Sunagawa (1984) and Perugini et al. (2008). On a microscale, the models show that relationships between the concentrations of two elements of different mobilities do not follow the pattern expected from the mixing of two end-member magmas. Differing mobilities and differing element exchange rates between mixed magma domains come into play as magmas of slightly differing compositions are chaotically advected to growing crystals during mixing. If the mobility rates for every element are different, linear correlations cannot apply to the concentrations of any two elements in active mixing domains and, as the active domains feed the growing crystal, the differences will be reflected in its composition. The models are complementary and open the possibility of assessing, at two different levels (general and detailed), the degree of element exchange and of magma blending between two magmas. The models also allow estimation of deviation from linear behavior by elements at different stages of mixing.

Acknowledgments The research was done within the framework of IGCP 510. We express our appreciation to D. Perugini, G. Poli and R. Macdonald for discussion on magma mixing processes. We are

grateful for all three very thoughtful reviews that enabled us to make our models more consistent and to interpret them better. We appreciate the friendly assistance by P. Kennan and R. Dymock who substantially improved the scientific content and who corrected both English style and grammar and J. Hoefs for efficient editorial oversight and very helpful comments.

Open Access This article is distributed under the terms of the Creative Commons Attribution Noncommercial License which permits any noncommercial use, distribution, and reproduction in any medium, provided the original author(s) and source are credited.

References

- Acosta-Vigil A, London D, Morgan GB VI (2005) Contrasting interactions of sodium and potassium with H₂O in haplogranitic liquidus and glasses at 200 MPa from hydration-diffusion experiments. *Contrib Mineral Petrol* 149:276–287
- Acosta-Vigil A, London D, Morgan GB VI (2006) Experiments on the kinetics of partial melting of a leucogranite at 200 MPa H₂O and 690–800°C: compositional variability of melts during the onset of H₂O-saturated crustal anatexis. *Contrib Mineral Petrol* 151:539–557
- Barbarin B (2005) Mafic magmatic enclaves and mafic rocks associated with some granitoids of the central Sierra Nevada batholith, California: nature, origin, and relations with the hosts. *Lithos* 80:155–177
- Bindeman IN, Davis AM (1999) Convection and redistribution of alkalis and trace elements during the mingling of basaltic and rhyolitic melts. *Petrology* 7:91–101
- Bonin B (2004) Do coeval mafic and felsic magmas in post-collisional to within-plate regimes necessarily imply two contrasting, mantle and crustal, sources? A review. *Lithos* 78:1–24
- Cherniak DJ (1996) Strontium diffusion in sanidine and albite, and general comments on Sr diffusion in alkali feldspars. *Geochim Cosmochim Acta* 60:503–543
- Cherniak DJ (2002) Ba diffusion in feldspar. *Geochim Cosmochim Acta* 66:1641–1650
- Cooper GRJ (2003) Feature detection using sun shading. *Comput Geosci* 29:941–948
- De Campos CP, Dingwell DB, Fehr KT (2004) Decoupled convection cells from mixing experiments with alkaline melts from Phlegrean Fields. *Chem Geol* 213:227–251
- De Campos CP, Dingwell DB, Perugini D, Civetta L, Fehr TK (2008) Heterogeneities in Magma Chambers: insights from the behavior of major and minor elements during mixing experiments with natural alkaline melts. *Chem Geol* 256:131–145
- De Campos CP, Perugini D, Ertel-Ingrisch W, Dingwell DB, Poli G (2010) Enhancement of magma mixing efficiency by chaotic dynamics: an experimental study. *Contrib Mineral Petrol*. doi:10.1007/s00410-010-0569-0
- De Rosa R, Donato P, Ventura G (2002) Fractal analysis of mingled/mixed magmas: an example from the Upper Pollara eruption (Salina Island, southern Tyrrhenian Sea, Italy). *Lithos* 65:299–311
- Ferrachat S, Ricard Y (1998) Regular vs. chaotic mantle mixing. *Earth Planet Sci Lett* 155:75–86
- Finch AA, Klein J (1999) The causes and petrological significance of cathodoluminescence emissions from alkali feldspar. *Contrib Mineral Petrol* 135:234–243
- Flinders J, Clemens JD (1996) Non-linear dynamics, chaos, complexity and enclaves in granitoid magmas. *Trans R Soc Edinb Earth Sci* 87:225–232

- Fourcade S, Allegre CJ (1981) Trace element behavior in granite genesis: a case study. The calc-alkaline plutonic association from Querigut complex (Pyrenees, France). *Contrib Mineral Petrol* 76:177–195
- Gagnevin D, Daly JS, Poli G, Morgan D (2005) Microchemical and Sr isotopic investigation of zoned K-feldspar megacrysts: insights into the petrogenesis of a granitic system and disequilibrium crystal growth. *J Petrol* 46:1689–1724
- García-Moreno O, Castro A, Corretgé LG, El-Hmidi H (2006) Dissolution of tonalitic enclaves in ascending hydrous granitic magmas: an experimental study. *Lithos* 89:245–258
- Giletti BJ (1991) Rb and Sr diffusion in alkali feldspars, with implications for cooling histories of rocks. *Geochim Cosmochim Acta* 55:1331–1343
- Ginibre C, Wörner G, Kronz A (2004) Structure and dynamics of the Laacher See magma chamber (Eifel, Germany) from major and trace element zoning in sanidine: a cathodoluminescence and electron microprobe study. *J Petrol* 45:2197–2223
- Graham CM, Elphick SC (1990) A re-examination of the role of hydrogen in Al-Si interdiffusion in feldspars. *Contrib Mineral Petrol* 104:481–491
- Graham CM, Elphick SC (1991) Some experimental constraints on the role of hydrogen in oxygen and hydrogen diffusion and Al-Si interdiffusion in silicates. In: Ganguly J (ed) *Diffusion and flow in minerals and fluids, advances in physical chemistry*, vol 8. Springer, New York, pp 248–285
- Hirschmann MM (2006) Water, melting, and the deep Earth H₂O cycle. *Annu Rev Earth Planet Sci* 34:629–653
- Holloway JR (1987) Igneous fluids. In: Carmichael ISE, Eugster HP (Eds.), *Thermodynamic modelling of geological materials: minerals, fluids and melts*. Mineral Soc Am Rev Mineral 17:211–233
- Holten T, Jamtveit B, Meakin P, Cortini M, Blundy J, Austrheim H (1997) Statistical characteristics and origin of oscillatory zoning in crystals. *Am Mineral* 82:596–606
- Kober B, Lippolt HJ (1985) Pre-Variscan mantle lead transfer to basement rocks as indicated by lead isotopes of the Schwarzwald crystalline, SW-Germany. II: lead isotope evolution of the European Hercynides. *Contrib Mineral Petrol* 90:172–178
- Kohlstedt DL, Bai Q, Wang Z-C, Mei S (2000) Rheology of partially molten rocks. In: Bagdassarov N, Laporte D, Thompson AB (eds) *Physics and chemistry of partially molten rocks*. Kluwer Academic Publishers, Dordrecht, pp 3–28
- Kouchi A, Sunagawa I (1984) A model for mixing basaltic and dacitic magmas as deduced from experimental data. *Contrib Mineral Petrol* 89:17–23
- Kronenberg AK, Yund RA, Rossman GR (1996) Stationary and mobile hydrogen defects in potassium feldspar. *Geochim Cosmochim Acta* 60:4075–4094
- Kusiak MA, Dunkley DJ, Słaby E, Budzyń B, Martin H (2008) U-Pb chronology of zircon from granites of the Karkonosze Pluton, NE Bohemian Massif. 4th SHRIMP workshop—abstract volume: June 29–July 4, 2008, VSEGEI, Saint-Petersburg, Russia, pp 78–80
- Kusiak MA, Dunkley DJ, Słaby E, Martin H, Budzyń B (2009) Sensitive high-resolution ion microprobe analysis of zircon reequilibrated by late magmatic fluids in a hybridized pluton. *Geology* 37:1063–1066
- Langmuir C, Vocke RDJ, Hanson GM, Hart SR (1978) A general mixing equation with application to the Icelandic Basalts. *Earth Planet Sci Lett* 37:380–392
- Liu M, Muzzio FJ, Peskin RL (1994a) Quantification of mixing in aperiodic chaotic flows. *Chaos Solutions Fractals* 4:869–893
- Liu M, Peskin RL, Muzzio FJ, Leong CW (1994b) Structure of the stretching field in chaotic cavity flows. *Am Inst Chem Eng J* 40:1273–1286
- Mandelbrot BB (1982) *The fractal geometry of nature*. W.H. Freeman, New York
- Marfunin AS, Bershov LV (1970) Electron-hole centers in feldspars and their possible crystallochemical and petrological significance (in Russian.). *Doklady Akademii Nauk* 193:412–414
- McCaughey JL (1993) *Chaos, dynamics and fractals: an algorithmic approach to deterministic chaos*. Cambridge University Press, Cambridge
- Mikulski SZ, Stein HJ (2007) Re-Os age for molybdenite from the West Sudetes, SW Poland. In: *Granitoids in Poland*, *Archiwum Mineralogiczne*, monograph no. 1, pp 203–216
- Mikulski SZ, Bagiński B, Dzierżanowski P (2004) The CHIME age calculation on monazite and xenotime in aplogranite from the Szklarska Poręba Huta quarry. *Polish Mineral Soc Spec Pap* 24:287–290
- Morgan GB, London D (2003) Trace-element partitioning at conditions far from equilibrium: Ba and Cs distributions between alkali feldspar and undercooled hydrous granitic liquid at 200 MPa. *Contrib Mineral Petrol* 144:722–738
- Morgan GB VI, Acosta-Vigil A, London D (2008) Diffusive equilibration between hydrous metaluminous-peraluminous haplogranite liquid couples at 200 MPa (H₂O) and alkali transport in granitic liquids. *Contrib Mineral Petrol* 155:257–269
- Ottino JM, Muzzio FJ, Tjahjadi M, Franjone JG, Jana SC, Kusch HA (1993) Chaos, symmetry, and selfsimilarity: exploiting order and disorder in mixing processes. *Science* 257:754–760
- Perugini D, Poli G (2004) Analysis and numerical simulation of chaotic advection and chemical diffusion during magma mixing: petrological implications. *Lithos* 78:43–66
- Perugini D, Poli G, Gatta GD (2002) Analysis and simulation of magma mixing processes in 3D. *Lithos* 65:313–330
- Perugini D, Poli G, Mazzuoli R (2003) Chaotic advection, fractals and diffusion during mixing of magmas: evidence from lava flows. *J Volcanol Geotherm Res* 124:255–279
- Perugini D, Poli G, Valentini L (2005) Strange attractors in plagioclase oscillatory zoning: petrological implications. *Contrib Mineral Petrol* 149:482–497
- Perugini D, Petrelli M, Poli G (2006) Diffusive fractionation of trace elements by chaotic mixing of magmas. *Earth Planet Sci Lett* 243:669–680
- Perugini D, De Campos CP, Dingwell DB, Petrelli M, Poli D (2008) Trace element mobility during magma mixing: preliminary experimental results. *Chem Geol* 256:146–157
- Petrov I (2002) Effective site symmetry of Fe³⁺ at aluminium positions in sodium, potassium and barium feldspar. <http://www.petrov.de>
- Pietranik A, Koepke J (2009) Interactions between dioritic and granodioritic magmas in mingling zones: plagioclase record of mixing, mingling and subsolidus interactions in the Gęsiniec Intrusion, NE Bohemian Massif, SW Poland. *Contrib Mineral Petrol* 158:17–36
- Poli G, Tommasini S (1991) Model for the Origin and Significance of Microgranular Enclaves in Calc-alkaline Granitoids. *J Petrol* 32:657–666
- Poli G, Tommasini S, Halliday AN (1996) Trace elements and isotopic exchange during acid-basic magma interaction processes. *Trans R Soc Edin Earth Sci* 87:225–232
- Ren M (2004) Partitioning of Sr, Ba, Rb, Y, and LREE between alkali feldspar and peraluminous silicic magma. *Am Miner* 89:1290–1303
- Sibson R (1981) A brief description of natural neighbor interpolation. In: Barnett V (ed) *Interpreting multivariate data*. Wiley, New York
- Słaby E (2005) CHARAC- non-CHARAC behaviour of Y/Ho and Zr/Hf in Karkonosze hybridic and granitic melts. *Polish Mineral Soc Spec Pap* 25:200–203

- Słaby E, Götze J (2004) Feldspar crystallization under magma-mixing conditions shown by cathodoluminescence and geochemical modelling—a case study from the Karkonosze pluton (SW Poland). *Mineral Magaz* 64:541–557
- Słaby E, Martin H (2008) Mafic and felsic magma interactions in granites: the Hercynian Karkonosze pluton (Sudetes, Bohemian Massif). *J Petrol* 49:353–391
- Słaby E, Michalik M, Mierzejewski M (2005) Zr-Y-HREE enriched granitic vein rock from Karkonosze (SW Poland)—record of early fractionation of crustal melt? *Polish Mineral Soc Spec Pap* 25:204–207
- Słaby E, Galbarczyk-Gąsiorowska L, Seltmann R, Müller A (2007a) Alkali feldspar megacryst growth: geochemical modelling. *Mineral Petrol* 68:1–29
- Słaby E, Seltmann R, Kober B, Müller A, Galbarczyk-Gąsiorowska L, Jeffries T (2007b) LREE distribution patterns in zoned alkali feldspar megacrysts—implication for parental melt composition. *Mineral Magaz* 71:193–217
- Słaby E, Götze J, Wörner G, Simon K, Wrzalik R, Śmigielski M (2008a) K-feldspar phenocrysts in microgranular magmatic enclaves: a cathodoluminescence and geochemical study of crystal growth as a marker of magma mingling dynamics. *Lithos* 105:85–97
- Słaby E, Martin H, Domonik A, Śmigielski M (2008b) Crystal growth in heterogeneous magmas—3D visualization and self-affine fractal statistics. *Geochim Cosmochim Acta* 72(12 suppl 1):A876
- Słaby E, Götze J, Wörner G, Simon K, Wrzalik R, Śmigielski M (2009) Order-disorder in K-feldspar grown from mixed magmas—CL and Raman study. Conference on micro-Raman spectroscopy and luminescence studies of the earth and planetary sciences (Corals I) April 2–4, 2009 Mainz, Germany, #3003
- Tepley FJ, Davidson JP, Tilling RI, Arth JG (2000) Magma mixing, recharge and eruption histories recorded in plagioclase phenocrysts from El Chichon Volcano, Mexico. *J Petrol* 41:1397–1411
- Viswanathan K, Brandt K (1980) The crystal structure of a ternary (Ba, K, Na)-feldspars and its significance. *Am Mineral* 65:472–476
- Viswanathan K, Kielhorn H-M (1983) Al, Si distribution in a ternary (Ba, K, Na)-feldspar as determined by crystal structure refinement. *Am Mineral* 68:122–124
- Waight TE, Maas R, Nicholls IA (2000) Fingerprinting feldspar phenocrysts using crystal isotopic composition stratigraphy: implications for crystal transfer and magma mingling in S-type granites. *Contrib Mineral Petrol* 139:227–239
- Yoeli P (1965) Analytical hill shading. *Surveying and Mapping* 25:573–579
- Žák J, Klomínský J (2007) Magmatic structure in the Krkonoše-Jizera Plutonic Complex, Bohemian Massif: evidence for localized multiphase flow and small-scale thermal—mechanical instabilities in a granitic magma chamber. *J Volcanol Geotherm Res* 164:254–267
- Žák J, Verner K, Týcová P (2008) Grain-scale processes in actively deforming magma mushes: new insights from electron backscatter diffraction (EBSD) analysis of biotite schlieren in the Jizera granite, Bohemian Massif. *Lithos* 106:309–322
- Žák J, Verner K, Klomínský J, Chlupáčová M (2009) “Granite tectonics” revisited: insights from comparison of K-feldspar shape-fabric, anisotropy of magnetic susceptibility (AMS), and brittle fractures in the Jizera granite, Bohemian Massif. *Int J Earth Sci* 98:949–967